"Word count: 9325"

Revision 2

Thermal metamorphic history of Antarctic CV3 and CO3 chondrites inferred from the first and second order Raman peaks of polyaromatic organic carbon.

Mehmet Yesiltas[1]*, Jordan Young[2], Timothy D. Glotch[2]

[1] Faculty of Aeronautics and Space Sciences, Kirklareli University, Kirklareli, Turkey 39100
[2] Department of Geological Sciences, Stony Brook University, Stony Brook, NY, USA 11794

* Corresponding author: myesiltas@knights.ucf.edu

Suggested Running Title: Thermal metamorphism of Antarctic CV3 and CO3 chondrites.

This is the peer-reviewed, final accepted version for American Mineralogist, published by the Mineralogical Society of America.
The published version is subject to change. Cite as Authors (Year) Title. American Mineralogist, in press.
DOI: https://doi.org/10.2138/am-2021-7507. http://www.minsocam.org/

ABSTRACT

Parent body thermal metamorphism is an important process that alters the structure of organic matter in the parent asteroid of meteorites. Increasing and progressing thermal metamorphism results in carbonization and graphitization of carbonaceous matter in the parent body. Such modifications in the carbon structures can be studied by Raman microspectroscopy, thanks to its high sensitivity to structure and bonding within carbonaceous molecules. We have characterized polyaromatic carbonaceous matter in a total of 24 Antarctic CV3 and CO3 chondrites using micro-Raman imaging spectroscopy in an effort to better understand parent body thermal metamorphism and assess its effects on the carbon structures. Raman spectral parameters of the first order carbon peaks (D and G) were extracted from at least 200 spectra for each meteorite and were compared to deduce relationships that yield information regarding the thermal metamorphism conditions. We also show, for the first time, spectral trends and relations of the second order carbon peaks (2D and D+G) within the 2500-3200 cm^{-1} with thermal metamorphic history. The second order peaks appear to contain information that is lacking in the first order peaks. Based on the second order carbon peak parameters, we tentatively classify four CV3 chondrites into subtypes, and reclassify another. Peak metamorphic temperatures of the investigated meteorites have been estimated based on the width of the D band as well as the calculated Raman spectral curvature. Estimated temperatures appear to correlate well with the assigned petrologic types. We have calculated higher peak metamorphic temperatures for the CV3 chondrites than for the considered CO3 chondrites and further showed that the peak metamorphic temperatures of $CV3_{oxA}$ chondrites are higher than those of $CV3_{oxB}$, indicating a possibly different metamorphic conditions for the two oxidized subtypes. We observe that there is a relatively larger temperature increase going from CO3.2 to CO3.4 (150 °C increase)

This is the peer-reviewed, final accepted version for American Mineralogist, published by the Mineralogical Society of America.
The published version is subject to change. Cite as Authors (Year) Title. American Mineralogist, in press.
DOI: https://doi.org/10.2138/am-2021-7507. http://www.minsocam.org/

compared to CO3.4-CO3.6 (20 °C), which may indicate that the graphitization and structural ordering of carbon reach a critical temperature regime around petrologic type CO3.3.

Keywords: Carbonaceous chondrites, Organic matter, Raman spectroscopy, Thermal metamorphism.

INTRODUCTION

Secondary processes such as aqueous alteration and thermal metamorphism take place on the parent asteroids of chondrites, and as a result the asteroidal compositions and components are subsequently modified at varying scales and intensities (Brearley and Jones, 1998; Krot et al., 2003; Huss et al. 2006). Thermal metamorphism is a relatively minor effect in carbonaceous chondrites with petrologic type 1 and 2, although these meteorites experienced sufficient heating to mobilize water, which in return initiated the aqueous alteration. Type 3 carbonaceous chondrites escaped elevated temperatures in the parent body that would potentially equilibrate the chemical compositions, however they still reached relatively higher temperatures than type 1 and 2 chondrites, which caused a wide range of compositional modifications including thermal processing of the organic matter (Brearley, 2006; Huss et al. 2006). On the other hand, type 4, 5, 6, and 7 carbonaceous chondrites experienced even higher temperatures such that their composition has been equilibrated (Ashworth, 1980; Kessel et al. 2007).

Some chondrites, especially carbonaceous chondrites, contain up to 4 wt.% organic carbon in the form of soluble and insoluble organic matter, the latter comprising about ~80% of the total organic carbon (Remusat, 2014). Secondary processes such as thermal metamorphism, aqueous alteration, brecciation, and impact shock can modify the organic content of chondrites (Botta and

Bada, 2002; Pizzarello et al. 2006). For instance, organic carbon in carbonaceous chondrites include polyaromatic macromolecular organic carbon, whose structures are sensitive to heating (i.e., thermal metamorphism) and elevated temperatures make them more graphitic (Busemann et al. 2007; Cody et al. 2008). Because carbonaceous chondrites are not differentiated, signatures of thermal metamorphism are preserved and retained in their chemical content (Scott and Krot, 2007), thus opening a path for investigating the asteroidal thermal metamorphism.

Carbonaceous chondrites exhibit a wide range of chemical diversity, and some variations exist as a result of asteroidal secondary processes (Zolensky et al. 1993). Ornans-type (CO) and Vigarano-type (CV) carbonaceous chondrites are petrologic type 3, referred to as CO3 and CV3 chondites (McSween, 1977a; Greenwood and Franchi, 2004; Weisberg et al. 2006). This means that they are among the least altered/modified chondrites (Krot et al. 2005). The CO3 chondrites contain abundant presolar silicates (Alexander et al. 2018). They show evidence of asteroidal metasomatic events, and the presence of melilite, plagioclase, nepheline, sodalite, ilmenite, ferroan olivine, and ferroan diopside have been identified (Brearley and Krot, 2013). The CV3 chondrites contain a wide range of secondary anhydrous minerals and some hydrous phases (Brearley and Krot, 2013). Ferroan olivine and diopside–hedenbergite solid solution pyroxenes, nepheline, sodalite, phyllosilicates and fayalite have been identified in most CV3 chondrites (MacPherson et al. 2014).

The CO3 chondrites are reported to be compositionally related to the CV3 chondrites. For instance the CO3 and CV3 chondrites have similar bulk chemical compositions and mineralogies (Itoh and Tomeoka, 2003) although their metal phases are quite different (McSween, 1977b,

1977c). The CO3 chondrites span a range of petrologic types, from 3.0 to 3.9 (McSween, 1977a; Keck and Sears, 1987), and as such, they provide an excellent set of samples to study parent body metamorphic processes. On the other hand, CV3 chondrites are divided into two subgroups; reduced ($CV3_{red}$) and oxidized ($CV3_{ox}$) chondrites on the bases of their secondary mineralogy and opaque phases such as metal, magnetite, and Ni content (McSween, 1977c). The oxidized subgroup ($CV3_{ox}$ chondrites) are further divided into the Allende-like ($CV3_{oxA}$) and Bali-like ($CV3_{oxB}$) types also on the bases of their secondary minerals and magnetite abundances (Weisberg et al. 1997b, Krot et al. 1998). In addition to the secondary minerals and magnetite abundances, thermoluminescence properties of CV3 chondrite subtypes are different as well (Guimon et al. 1995). Another difference among the CV3 subtypes is the varying abundances of pure fayalite. Namely, the CV_{oxA} subtypes lack pure fayalite (Fa>95 composition) and it is rare in the $CV3_{red}$ subtypes, whereas relatively larger amounts exist in the $CV3_{oxB}$ subtypes (McSween et al. 1977c; Howard et al. 2010). While these CV3 subtypes were thought to originate from a single parent body, there are mineralogical differences among the three subgroups due to varying degrees of alteration (Krot et al., 1995, 2003). In fact, on the basis of significantly different matrix abundances and the distribution of chondrule apparent diameters, it was argued that the CV_{ox} and CV_{red} chondrites may originate from two different parent bodies (Gattacceca et al. 2019). If true, it would be interesting to compare their thermal metamorphic histories, which can be investigated via Raman spectroscopy of the polyaromatic carbonaceous matter within the CV3 chondrites. Indeed, due to the relatively low degree of thermal processing in the CO3 and CV3 chondrites (Itoh and Tomeoka, 2003; Alexander, 2017), the study and comparison of their carbon structures may provide valuable information regarding the parent body metamorphism mechanisms.

125

126 To investigate the effects of parent body thermal metamorphism on polyaromatic carbonaceous
127 matter and to compare these effects across the two chondrite groups, we collected Raman
128 spectroscopic data from a set of Antarctic CO3 and CV3 chondrites, and extracted spectral
129 parameters of the first and second order carbon peaks. The first order carbon peaks have been
130 previously studied and spectral trends have been presented for various carbonaceous chondrite
131 groups (Bonal et al. 2006, 2007; 2016, 2020, Busemann et al. 2007; Cody et al. 2008; Quirico et
132 al. 2018), however, to our knowledge, the second order carbon peaks have not been investigated.
133 In this work, these second order carbon peaks were strong enough to consider and investigate
134 them, so these peaks and their parameters were also taken into account, for the first time, in an
135 effort to reveal relations between the organic matter and thermal metamorphic histories. We also
136 show that spectral trends and parameters of the second order carbon peaks may able to recognize
137 the subtypes of CV3 chondrites. Using such parameters, we attempt to tentatively classify four
138 carbonaceous chondrites and reclassify another into the CV3 subtypes.

139

140 **SAMPLES AND ANALYTICAL METHODS**

141 The CO3 and CV3 chondrites studied in this work were loaned in the form of polished thin
142 sections from the Antarctic meteorite collection of NASA Astromaterials Acquisition and
143 Curation Office located at Johnson Space Center (JSC). At JSC, each sample was first cut dry on
144 a band saw, producing a ~cm scale thick slab, which was then glued on a glass slide using epoxy
145 for further processing using diamond paste to make the section ~30-40 μm thin, flat and smooth.
146 Table 1 lists the studied samples and their types. While the subtypes of most samples are known,

147 there are four CV3 and three CO3 chondrites whose subtypes are currently unknown. These
148 samples are indicated by "?" in the associated figures and tables.
149
150 Meteoritic components are susceptible to chemical modifications in the field and in the
151 laboratory. For instance, terrestrial weathering may alter the organic matter in meteorites,
152 especially those found in hot deserts (Busemann et al. 2007, Alexander et al. 2007). Meteorites
153 found in cold deserts such as Antarctica, on the other hand, remain relatively more pristine. The
154 samples investigated in this work all have A or B terrestrial weathering grades, indicating
155 minimal weathering. Additionally, organic contamination in the laboratory may occur during
156 sample preparation, however contaminant organics present Raman peaks that are different to
157 some extent than indigenous carbon and are easily identifiable. Epoxy resin used during the
158 sample preparation can also give rise to contaminant Raman carbon peaks, however these peaks
159 are quite distinct from those of indigenous carbonaceous matter, therefore they can be easily
160 distinguished (e.g., Yesiltas, 2018a). Nevertheless, all spectra included in the data analyses were
161 checked prior to fitting procedures to ensure all investigated spectra are free of contaminant
162 carbon peaks.
163
164 Our samples were prepared in the form of thin sections, which involved polishing the surface of
165 samples. Such mechanical polishing processes might introduce structural disruption on the
166 organic matter present on the surface (Beyssac et al., 2003; Fries and Steele, 2010); however,
167 type 3 chondrites reportedly did not contain structural modifications due to the polishing (Bonal
168 et al. 2016). Nevertheless, extra caution was taken during the data collection and analyses
169 procedures of this work. In order to check whether polishing causes changes in the Raman

spectral parameters, we measured a polished thin section, powdered grains, and bulk chip of a type 3 carbonaceous chondrite. Spectral results in all cases appear very similar, indicating that the effect of surface polishing in this work should be negligible.

Table 1. Meteorite samples investigated in this study.

Number*	Meteorite	Group/Subtype
1	ALH 85006	$CV3_{oxB}$
2	MET 00430	$CV3_{oxB}$
3	LAR 06317	$CV3o_{xA}$
4	DOM 10351	CV3?
5	MCY 05219	$CV3_{oxB}$
6	MIL 13328	CV3?
7	QUE 93744	CV3?
8	LAP 02228	$CV3_{oxA}$
9	LAP 02206	$CV3_{oxA}$
10	MIL 07681	$CV3_{red}$
11	LAR 12002	CV3?
12	GRA 06101	$CV3_{oxA}$
13	DOM 08006	CO3.0
14	MIL 090152	CO3.?
15	MIL 090128	CO3.0-3.2
16	MIL 11213	CO3.?
17	MIL 07193	CO3.1
18	MIL 05024	CO3.1
19	MIL 090010	CO3.1
20	DOM 10104	CO3.2
21	MIL 07346	CO3.2
22	ALH 82101	CO3.4
23	ALH 83108	CO3.5
24	ALHA 77003	CO3.6

*The numbers denote sample numbers in the legends of figures.

Raman microspectroscopy experiments were conducted using a WiTec alpha300R confocal Raman imaging system (WiTec GmbH), which was equipped with a 532 nm Nd:YAG laser, 600 g/mm grating, and a 50× (NA = 0.8) objective. The laser power on the focal plane (sample surface).was ~1-1.5 mW (corresponding to a power density of ~0.57-0.85 mW/μm^2), which appears to cause no laser-induced thermal damage on the sample. Prior to each measurement

session, the spectrograph was calibrated using a silicon wafer substrate to ensure the Rayleigh laser signal was at 0 cm^{-1} and the signal of silicon was at ~521 cm^{-1}. Following the calibration, we collected two-dimensional Raman images from a carbon-bearing region of each sample with 0.5 μm spatial step size. The data collection procedure was automatic, as the confocal microscope raster scanned the predefined area pixel by pixel and acquired a Raman spectrum between the whole spectral range (0-4000 cm^{-1}) from all pixels, covering the first and second order carbon peaks. The resulting hyperspectral images consist of thousands of pixels each with its lateral information and a full Raman spectrum. Integration time was between 0.03-0.09 s. These parameters proved to generate reproducible spectral data with no laser-induced damage to the studied samples (e.g., Yesiltas et al. 2018a, 2018b; Yesiltas et al. 2019).

The collected data were first corrected for cosmic rays and artificial baseline (by subtracting a polynomial with shape size of 200 and noise factor of 2). Next, carbon distribution maps were generated for each sample to identify the carbon-rich pixels. Figure 1 presents these distribution maps for the 24 meteorites investigated in this study. We fitted the first order carbon peaks with a pair of Lorentzian functions and extracted width (Γ), intensity (I), and position (ω) of each carbon peak. Such a fitting procedure was repeated for at least 200 carbon-rich pixels in each sample, which ensures that the spectral data are representative of the whole sample and any sampling bias is minimized. The same spectral parameters were also extracted from the second order carbon peaks of average meteorite spectra. The extracted parameters were then plotted against each other to obtain spectral trends and relations which could help us infer thermal metamorphic history of the parent bodies of the samples and relationships across a range of petrologic subtypes of the CV3 and CO3 chondrites.

This is the peer-reviewed, final accepted version for American Mineralogist, published by the Mineralogical Society of America.
The published version is subject to change. Cite as Authors (Year) Title. American Mineralogist, in press.
DOI: https://doi.org/10.2138/am-2021-7507. http://www.minsocam.org/

RESULTS

Average baseline-corrected Raman spectra of investigated meteorite samples are shown in Figure 2. Carbonaceous matter generally produces first and second order carbon peaks. The first order peaks occur between 1000-1800 cm^{-1} and are present in spectra of all samples considered in this work. These peaks specifically appear near ~1350 and ~1600 cm^{-1}. The former peak is referred to as the "D" (disorder) band and is due to sp^3 carbon bonding (Busemann et al. 2007; Suzuki et al. 2010). It occurs due to the breathing motion of sp^3 atoms in rings, and as a result of defects in the carbon structures (Tuinstra and Koenig 1970; Ferrari and Robertson 2000, 2001, Starkey et al. 2013). The latter band is referred to as the "G" (graphite) band and is due to sp^2 carbon bonding (Tuinstra and Koenig 1970; Busemann et al. 2007; Suzuki et al. 2010). The G band occurs as a result of in-plane stretching mode of sp^2 atoms in polyaromatic rings, and different types of carbonaceous materials can be distinguished using the spectral properties of this band (Ferrari and Robertson 2000, 2001, Starkey et al. 2013). The second order carbon peaks, which appear at higher wavenumbers between 2500-3500 cm^{-1}, are overtones and combinations of the first order peaks (Sadezky et al. 2005, Brunetto et al. 2009). The 2D peak appears around ~2700 cm^{-1} and is the overtone of the D band (Vollebregt et al. 2012; Ma et al. 2019), whereas the peak near ~2930 cm^{-1} is called the D+G band and is the overtone of the D and G bands (Vollebregt et al. 2012; Ma et al. 2019). The vertical dashed lines at 1343, 1600, 2690, and 2930 cm^{-1} in Figure 2 indicate positions of the D, G, 2D and D+G bands observed in this work.

By fitting the first order carbon peaks with various mathematical functions, spectral peak parameters such as full-width-half-maxima (Γ), peak intensity (I), and peak position (ω) can be extracted (e.g., Bonal et al. 2006, 2007; 2016, 2020, Busemann et al. 2007; Cody et al. 2008; Quirico et al. 2018). In this study, we extracted spectral parameters of the first order carbon peaks from at least 200 Raman spectra for each meteorite by fitting the peaks with a pair of Lorentzian functions (Figure 3). As for the second order carbon peaks, we extracted the same spectral peak parameters from the average Raman spectra given in Figure 2. The values of individual parameters (given in Table S1-supplementary file) were compared across all of the considered samples in order to obtain useful information to understand the thermal metamorphism that occurred on their respective parent bodies and also to assess whether the second order peak parameters provide any trend or relation that could be useful for constraining the thermal metamorphic history.

Figure 4a shows that the peak intensity ratio (I_D/I_G) of first order carbon peaks increases with increased thermal metamorphism. Namely, DOM 08006 (CO3.0, characterized by the most disordered organic matter) has a I_D/I_G ratio of 0.77, whereas relatively more ordered DOM 10104 (CO3.2) and ALHA 77003 (CO3.6) are characterized by I_D/I_G ratios of 1.0 and 1.34, respectively. This is due to the fact that there are two phases of thermal metamorphism; a carbonization phase that contributes disordered aromatic carbon to the D peak, and a higher temperature graphitization phase that reduces the D peak. In addition, the observed trend (increasing ratio as a result of increased thermal metamorphism) has been attributed to the transformation of amorphous carbon to relatively crystalline carbon (i.e., nanocrystalline graphitic domains) and then to inorganic graphite (Tuinstra and Koenig 1970; Ferrari and

Robertson, 2000, 2001; Busemann et al. 2007). The comparison in Figure 4a also shows that the Γ_D value decreases with increasing petrologic type as expected. These trends are consistent with higher petrologic types being the result of increased temperatures in the parent body (Huss et al. 2006). Moreover, these trends indicate that the considered CO3 chondrites are more primitive with more amorphous and disordered carbon, whereas the CV3 chondrites appear to have experienced relatively higher levels of thermal metamorphism. While some samples show signs of presence of relatively crystalline carbon, the complete transformation to inorganic graphite is not observed in the studied samples because there is no Raman spectrum that shows prominently strong G band and relatively weak or almost absent D band, which is the indication of inorganic graphite (e.g., Busemann et al. 2007). On the other hand, the I_D/I_G ratio does not present any relation with Γ_G (Figure 4b), indicating that transformation of carbon from amorphous to nanocrystalline structure may have no visible effect on the width of the G band based on the samples studied here.

Figure 5a shows that the position of the D-band (ω_D) spans a similar range for both groups of meteorites, however the D-band width (Γ_D) is generally greater for CO3 chondrites than for CV3 chondrites. The greater D-band widths for CO3 chondrites suggest the presence of relatively disordered carbon and less metamorphism than CV3 chondrites. In addition, the three $CV3_{oxA}$ chondrites (samples 8, 9, 12) plot at lower Γ_D values compared to the three $CV3_{oxB}$ chondrites (samples 1, 2, 5), suggesting that the former subtypes may have undergone relatively higher degree of thermal metamorphism. Figure 5b presents the same parameters (peak position vs. peak width) for the G-band. These two parameters, ω_G as a function of mean crystallite size and Γ_G as a function of the distribution of crystallite size, were previously used to describe the

thermal metamorphism of carbonaceous chondrites (e.g., Busemann et al. 2007; Jenniskens et al. 2012; Bonal et al. 2016). In this work, we see that CV3 chondrites fall toward lower right in this graph, indicating the presence of polycrystalline and metamorphosed organic matter in CV3 chondrites. The reduced and oxidized CV3 chondrites plot randomly with no apparent grouping, indicating that these band parameters are unable to differentiate different CV3 subgroups. CO chondrites fall below CM chondrites in this figure, showing an agreement with the previous work (e.g., Busemann et al. 2007; Jenniskens et al. 2012; Bonal et al. 2016), but they span a large range such that some CO3 chondrites extend into to the CV region, which is indicative of material in those CO3s that has been metamorphosed as much as the considered CV chondrites.

The width of the D band (Γ_D) is positively correlated with the width ratio of D and G bands (Γ_D/Γ_G), as shown in Figure 6a. Increasing the degree of thermal metamorphism appears to decrease the Γ_D value, but does not seem to affect Γ_G at all. Relatively more metamorphosed members of the CO chondrites (types 3.4-3.6) fall in the middle of CV chondrites in this graph. Unlike Γ_D, the Γ_G parameter does not seem to have any correlation to the width ratio Γ_D/Γ_G (Figure 6b), except that the two groups of meteorites cluster slightly apart from each other. Moreover, we show that some of the spectral properties of the first order carbon peaks do not present any trend. For instance, the position of the D band does not seem to be an indicator of metamorphism as the position values for all meteorites are scattered randomly (Figure S1). Comparisons of peak widths (Γ_D vs. Γ_G) as well as positions (ω_D vs. ω_G) do not reveal any trend that can be related to the parent body thermal metamorphism (Figure S2). Figure 7 presents the I_D/I_G ratios for the investigated meteorites. CV3 chondrites appear to follow a linear trend, the

comparison indicates that $CV3_{oxB}$ chondrites have smaller I_D/I_G ratios than $CV3_{oxA}$ chondrites. The I_D/I_G ratios of CO3 chondrites also appear to increase with increasing petrologic types.

Spectral parameters of the second order carbon peaks could be valuable for understanding the maturity grade (Bonal et al. 2007). Yet, to our knowledge, these peaks have not been previously studied quantitatively for the purpose of understanding parent body thermal metamorphism such as the parent bodies of CV and CO chondrites. Average Raman spectra in this work have high enough signal-to-noise ratio within the 2500-3500 cm^{-1} region such that we are able to perform fitting procedures to extract spectral parameters from the second order carbon peaks. We investigated these second order peaks to explore their potential for this purpose and to check whether they are able to distinguish different petrologic subtypes. Figure 8a shows a linear relationship between Γ_{2D} and Γ_{2D}/Γ_{D+G}, which is very similar to the trend seen in Figure 6a for the same parameters of first order peaks (Γ_D vs. Γ_D/Γ_G), although both meteorite groups span similar ranges with no obvious distinction between the CO3 and CV3 chondrites in Figure 8a. What is additionally observed in Figure 8a is that the width of the 2D band for $CV3_{oxA}$ chondrites (samples 8, 9, 12) appears to be similar and is located near 75-100 cm^{-1}, however the value of this parameter is much larger (200-275 cm^{-1}) for the $CV3_{oxB}$ chondrites (samples 1, 2, 5), therefore they are spectrally separated based on the second order carbon peak parameters. A similar trend is also seen in the right panel of this figure. The $CV3_{oxA}$ chondrites generally have higher peak intensity ratios than the $CV3_{oxB}$ chondrites, with the exception of LAR 06317 (see text below). Figure 8b shows that Γ_{2D} decreases and I_{2D} increases as thermal metamorphism progresses. In this case, one must expect a linear relation between Γ_{2D} and I_D as well, which is indeed what's seen in our data (Figure 9a). Thanks to the second order peak parameters, we

316 observe that while the I_D/I_G parameter does not present any trend or relationship with Γ_G, it does
317 have a linear relation with a second order peak parameter Γ_{D+G} (Figure 9b). Moreover, we
318 observe that the position of the D+G band (ω_{D+G}) is linearly correlated with the Γ_D value (Figure
319 10a), shifting to higher wavenumbers as metamorphism increases. This is in contrast to the first
320 order peaks, where increased metamorphism does not seem to vary the peak position ω_D. We
321 also observe that the three CV3 subtypes appear to plot separately when the I_{2D}/I_{D+G} values of the
322 considered CV3 chondrites are compared (Figure 10b), revealing that the I_{2D}/I_{D+G} values could
323 potentially be useful for distinguishing the three CV3 subtypes (see Discussion).
324
325 It has been proposed in the literature that Raman spectral parameters of the first order carbon
326 bands can be used to roughly estimate the peak metamorphic temperature (PMT) of parent
327 asteroids. For instance, Busemann et al. (2007) investigated insoluble organic matter (IOM) that
328 was chemically extracted from the matrices of primitive chondrites, and reported that the D band
329 parameters and peak metamorphic temperatures are strongly correlated, allowing for an
330 estimation of metamorphic temperatures using equation (1). However, this metamorphic
331 geothermometer is limited to samples with Γ_D values smaller than 280 cm^{-1} because the
332 minimum in the second order polynomial fit occurs at this value (Busemann et al. 2007). Cody
333 et al. (2008) reported an alternative geothermometer expression for the estimation of
334 metamorphic temperatures based on Γ_D (equation 2), realizing that there exists a relationship
335 between Γ_D and Raman exciton intensity. Cody et al. (2008) also reported a geothermometer
336 thermometer expression based on Γ_G (equation 3). However, the metamorphic temperatures
337 calculated using eq. 2 and 3 differ significantly, indicating that estimating the parent body
338 metamorphic temperature using Raman spectroscopy of polyaromatic carbon may be more

complicated than previously thought. Bonal et al. (2016) concluded that the peak metamorphic temperature calculations in the absence of a valid and consistent calibration procedure would not yield accurate results. In other words, the obtained temperatures could simply be underestimated without a proper calibration procedure. In addition, the thermometer expressions by Busemann et al. (2007) and Cody et al. (2008), used to estimate the structural order and maturity level of carbon in chondrites, are based only on one spectral parameter, the width of a first order carbon peak (either D or G band). Recently, Young et al. (2020) reported an alternative geothermometer model that is based on the calculated spectral curvature (K_T) of a given full Raman spectrum with D and G carbon bands (equation 4). This model, therefore, takes into account all parameters of both of the first order Raman peaks at the same time.

$$\text{PMT (°C)} = 931 - 5.10\times\Gamma_D + 0.0091\times\Gamma_D^2 \quad (1)$$

$$\text{PMT (°C)} = 899.9 - 3\times\Gamma_D + 0.0014\times\Gamma_D^2 \quad (2)$$

$$\text{PMT (°C)} = 1594.4 - 20.4\times\Gamma_G + 0.058\times\Gamma_G^2 \quad (3)$$

$$\text{PMT (°C)} = 0.409\times(-K_T^{-0.840}) \quad (4)$$

Even though the peak metamorphic temperatures obtained through these geothermometer expressions are somewhat underestimated due to their respective limitations, the Raman spectral parameters of first order carbon peaks and obtained temperatures nevertheless proved to be helpful for gaining insights on the thermal metamorphic history of parent asteroids (e.g., Bonal et al. 2016, 2020; Busemann et al. 2007; Cody et al. 2008; Yesiltas et al. 2014; Young et al. 2020).

We calculated the PMT values of the investigated meteorites using the expressions provided by Busemann et al. (2007), Cody et al. (2008), and Young et al. (2020), and compared the results of these models. The estimated PMT values obtained by different models yield similar trends with

363 respect to petrologic types of the samples, although each model estimates slightly different PMT
364 (Figure 11). Among the three models, the model by Cody et al. (2008) yields the highest
365 temperatures for the same samples. There is an average difference of ~93 °C between the Cody
366 et al. (2008) and Busemann et al. (2007) models. On the other hand, Young et al. (2020) model
367 estimates slightly higher temperatures for the type 3.0-3.2 CO chondrites, when compared with
368 the model of Busemann et al. (2007). Regardless of the thermometry models, the CO3 chondrites
369 present a lower range of temperatures than the CV3 chondrites. We note that for the PMT
370 calculations presented here, the equations based on Γ_D were used because the petrologic types of
371 the samples present better correlations with D band parameters (e.g., Busemann et al. 2007;
372 Bonal et al. 2007, Yesiltas et al. 2014; Bonal et al. 2020) and the spectral parameters of the D
373 band are reported to be more sensitive to annealing in the parent body (Busemann et al. 2007;
374 Bonal et al. 2007). We additionally compared the K_T values of our CV3 subtypes in an effort to
375 check whether the calculated spectral curvature values for the CV3 subtypes plot differently.
376 Figure 12 shows that the K_T values may potentially distinguish the CV3 subtypes as samples of
377 each subtype plot at different locations. In particular, investigated $CV3_{oxA}$ and $CV3_{oxB}$ chondrites
378 are separated as far as their K_T values are concerned. While the distinctions are not very
379 prominent in our case due to the limited number of samples, it would potentially be more
380 prominent when the spectral curvature values of a larger number of meteorites from each subtype
381 are compared.
382
383 **DISCUSSION**
384 Polyaromatic organic carbon structures in meteorites are sensitive to heating as the thermal
385 metamorphism induces irreversible structural/compositional transformations in the organic
386 matter (Bonal et al. 2006). As a response to thermal metamorphism, the Raman spectral

parameters of carbon peaks change accordingly (Busemann et al., 2007, Cody et al., 2008; Quirico et al., 2003; Bonal et al., 2006, 2007, 2016). Several groups focused on the first order carbon peaks and spectroscopically investigated the relations between carbon peak parameters and thermal metamorphism for various groups of meteorites (e.g., Busemann et al., 2007, Cody et al., 2008; Quirico et al., 2003; Bonal et al., 2006, 2007, 2016). First order carbon peak parameters of some of the samples investigated in this work were also studied by other groups in the past. Bonal et al. (2016) especially studied the first order carbon peaks of a large number of samples. Our investigation shows that increased thermal metamorphism results in a more intense and narrower D band with no change in its spectral position. On the other hand, the G band parameters are observed to be scattered randomly regardless of their petrologic types, and they do not vary in any systematic manner with thermal metamorphism. This is why the D band is favored for the calculation of peak metamorphic temperate of chondrites as the G band does not correlate significantly with thermal metamorphism (e.g., Busemann et al. 2007; Bonal et al. 2007, 2016). In short, our first order spectral peak parameters and their trends with thermal metamorphism are in good agreement with the literature (e.g., Quirico et al., 2003; Bonal et al., 2006, 2007, 2016; Busemann et al. 2007, Cody et al. 2008).

To our knowledge, the second order carbon peaks have not been quantitatively explored for the purpose of inferring thermal metamorphic history of carbonaceous chondrites. This may be due to low S/N ratio within the 2500-3500 cm^{-1} spectral region where the second order carbon peaks normally appear (e.g., Bonal et al. 2007). Sample type, sample form (powder vs. thin section), surface topography of the measured region (presence of voids or gaps), and experimental details can contribute to the obtained S/N level. We performed Raman imaging experiments on polished

thin sections, and considered hundreds of spectra from void-less regions to maximize the spectral quality. In our work, the second order carbon peaks are pronounced with high-enough S/N ratio that allows quantitative spectral investigations. Thanks to the high S/N ratio of our Raman spectra, we present spectral evidence, for the first time, that the second order carbon peak parameters may be used to infer parent body thermal metamorphism of carbonaceous chondrites, and also to potentially classify CV3 chondrites into its subtypes. These evidences are as follows:

(i) The spectral parameters extracted from the second order carbon peaks show that increased thermal metamorphism results in more intense and narrower 2D bands. We also show that the second order D+G peak near 2930 cm^{-1} does in fact present a correlation with thermal metamorphism, in contrast to the G band. Therefore, we conclude that it might be better to include the second order carbon peaks in the thermometric expressions/calculations to determine more accurate and better constrained peak metamorphic temperatures.

(ii) The second order peak parameters may also play a role in classifying subtypes of CV3 chondrites. For instance, the subtypes of CV3 chondrites ($CV3_{oxA}$, $CV3_{oxB}$, and $CV3_{red}$) present a unique challenge for understanding the parent body processes. The three subtypes may have gone through different extents of thermal metamorphism (Huss et al. 2006; Bonal et al. 2020). The $CV3_{oxA}$ chondrites present evidence of metasomatism, whereas the $CV3_{oxB}$ chondrites experienced substantial aqueous alteration (Huss et al. 2006). Bonal et al. (2020) reported that the $CV3_{oxA}$ chondrites contain higher abundance of metal and lower Ni in sulfides, while they have similar abundance of matrix. The $CV3_{red}$ chondrites present signatures of either aqueous alteration or metasomatism (Krot et al., 1995, Huss et al. 2006), they contain less matrix, more metal and Ni-poor sulfides relative to the oxidized CV3 chondrites (Bonal et al. 2020). Moreover, although it is thought that all CV3 chondrites originate from the same parent body,

Gattacceca et al. (2019) argued that $CV3_{ox}$ and $CV3_{red}$ chondrites may have originated from two different parent bodies. Bonal et al. (2020) also concluded that $CV3_{red}$ and $CV3_{ox}$ may be originating from the a heterogeneous parent body or multiple parent bodies on the bases that the two subtypes present different matrix abundances, alteration products, and opaque mineralogy. Despite the limited number of samples, we spectrally compared the three subtypes of CV3 chondrites based on their Raman spectra and peak parameters. Our data suggest that the samples of individual subtypes cluster together, and appear distant from other subtypes. The color-coded groups in Figure 10b correspond to the three CV3 subtypes in this work. The cyan group has average I_{2D}/I_{D+G} value of ~1.1 and contains three $CV3_{oxB}$ chondrites (samples 1, 2, and 5), three currently unclassified CV3 chondrites (samples 4, 6, and 7), and a $CV3_{oxA}$ (LAR 06317, see discussion below). The green group is composed of $CV3_{oxA}$ chondrites and presents a higher ratio (an average I_{2D}/I_{D+G} value of ~2.6). The only $CV3_{red}$ chondrite (sample 10) falls in close proximity to the green ($CV3_{oxA}$) group, while currently unclassified sample 11 presents the highest I_{2D}/I_{D+G} ratio. In this context, we can also attempt to anticipate the subtypes of samples 4, 6, 7, and 11. Based on Figures 8, 10, and 12, the CV3 samples 4, 6, and 7 can be tentatively classified into $CV3_{oxB}$, while sample 11 can be tentatively classified into $CV3_{red}$. On the other hand, the only reduced CV3 chondrite (sample 10) falls near the $CV3_{oxA}$ group in Figure 10, and should be further checked to verify its subtype.

(iii) Even though LAR 06317 was classified as $CV3_{oxA}$ (Lunning et al. 2016), it always plots together with the more primitive, less metamorphosed $CV3_{oxB}$ chondrites in our work when the second order carbon peak parameters are compared. While it is currently unknown why this is the case, one possibility might be the impact history of this particular meteorite in the parent body. In general, short term thermal metamorphism due to impacts and shock heating can affect

456 the structures of polyaromatic organic matter (i.e., ordering of carbon) (Quirico et al. 2018;
457 Nemeth and Garvie, 2020). Shock effects of impacts can also convert carbonaceous matter to
458 diamond (Nemeth and Garvie, 2020). As a result, impacts can complicate the effects of thermal
459 metamorphism in meteorites. The parent body of LAR 06317 may have experienced impacts and
460 collisions that caused shock heating of LAR 06317, as evidenced by the presence of multiple a
461 few mm-long impact melt clasts in the LAR 06317 (Lunning et al. 2016). In addition, while LAR
462 06317 has a shock grade of S3, Lunning et al. (2016) reported that LAR 06317 may have been
463 derived from precursors that had experienced only low-temperature thermal metamorphism.
464 Despite the impact history of LAR 06317, the polyaromatic organic matter appears to remain
465 more primitive than other CV_{oxA} chondrites. Another possibility could be the misclassification of
466 its subtype. Lunning et al. (2016) reported that LAR 06317 is a brecciated, oxidized Allende-
467 type CV3.5-3.9 (CV_{oxA}) chondrite, however Bonal et al. (2020) classified it as a CV_{oxB} based on
468 the modal abundance of metal and the average Ni content of sulfides. In our work, LAR 06317
469 always plots with $CV3_{oxB}$ chondrites in the second order peak parameter domains. Especially in
470 Figure 10b, LAR 06317 plots together with other $CV3_{oxB}$ chondrites, whereas the $CV3_{oxA}$
471 subtypes plot separately and further up in the I_{2D}/I_{D+G} parameter domain. Therefore, we
472 conclude, based on our Raman investigation, that LAR 06317 is more compatible with $CV3_{oxB}$
473 chondrites. We emphasize that the identification of LAR 06317 as $CV3_{oxB}$ is not clear when the
474 first order peak parameters are considered. This can suggest either LAR 06317 is in fact a
475 shocked $CV3_{oxA}$ but its polyaromatic organic matter structures remain primitive such that its
476 second order peak parameters still plot with $CV3_{oxB}$ while the first order parameters are unable to
477 distinguish it from $CV3_{oxA}$, or alternatively LAR 06317 is actually $CV3_{oxB,}$ in which case the
478 second order peak parameters again recognize this misclassification.

479

480 The peak metamorphic temperatures of the considered $CV3_{oxB}$ are calculated to be between 220 -
481 510 °C, however PMTs for $CV3_{oxA}$ vary from 450 °C to ~636 °C, indicating that studied $CV3_{oxB}$
482 chondrites are less metamorphosed (thus more primitive) than $CV3_{oxA}$ chondrites. This is in
483 agreement with the literature (e.g., Bonal et al. 2020). Furthermore, our data show a large
484 temperature increase (150 °C) between the CO3.2 and CO3.4 petrologic types, but much less
485 difference between CO3.4 and CO3.6 (20 °C), as shown in Figure 11. This may indicate that
486 during the thermal metamorphism, the graphitization and/or aromatization rate of carbon
487 structures in the CO3 chondrites initially proceeds at a higher rate but then the rate slows down
488 perhaps at a critical temperature regime/threshold where the carbonaceous matter reaches a
489 certain level of maturity and structural ordering of carbon.

490

491 Other processes such as ion irradiation in space can cause amorphization of carbon as well, and
492 as a result the G band's position moves towards lower wavenumbers (Busemann et al. 2007).
493 This may complicate the study of parent body thermal metamorphism based on Raman peak
494 parameters of carbon, because the irradiated carbonaceous matter in such meteorites would
495 appear closer to that of more primitive samples, implying relatively less thermal metamorphism.
496 However our Raman data show that there is no meteorite whose G band position is at such low
497 wavenumbers (i.e., no G band is present below 1595 cm^{-1}), therefore our results and implications
498 for the thermal history of investigated meteorites are free of complications introduced by the
499 external processes such as irradiation.

500

Understanding effects of asteroidal processes on organics may be more complex than previously thought. For instance, origin and starting materials of carbon may be different, and thermal metamorphism may cause different levels of ordering for carbon (Sears 2016). Two of the possible sources for the parent body thermal metamorphism are (i) long term heating (heating over a few million years) due to the decay of radionuclides such as ^{26}Al, and (ii) short term heating (a few days) due to impacts (Rubin et al. 1995; Nakato et al. 2008). The peak metamorphic temperature calculations assume the former, long term, heating in the parent body (Busemann et al. 2007). Possible effects of short term heating (such as impact heating) on the carbon structures are yet to be fully understood, and require additional work.

It is appropriate to note that while our results show trends and correlations between the carbon peak parameters and thermal metamorphism, they are not representative for the entire CV and CO group members. The small number of samples from each of the petrographic subtypes could reflect sampling biases. For instance, the three carbon thermometry equations yield roughly similar PMT ranges even though the models of Busemann et al. (2007) and Cody et al. (2008) are based only on Γ_D while the model of Young et al. (2020) is based on both Γ_D and Γ_G. In this case the Γ_G may seem to be a poor thermal metamorphism tracer; however, this may not necessarily be true because our results in this work may be affected by the sampling bias. More meteorites from various types should be studied to see the differences of the carbon thermometry models and how the parameters of the G band effects the PMT values.

IMPLICATIONS

523 Constraining the parent body processes is essential for understanding the early solar system and
524 its evolution. Detailed Raman spectral trends and relationships of polyaromatic carbonaceous
525 matter in a number of CV3 and CO3 chondrites were investigated in this work in an effort to (i)
526 infer the effects of parent body thermal metamorphism on the organic matter, (ii) check whether
527 the second order peak parameters can unravel any spectral relations with thermal metamorphism,
528 (iii) assess the capability and potential of the second order carbon peak parameters for classifying
529 the CV3 chondrites into one of its subtypes. We studied at least 200 spectra from each type 3
530 chondrite, and extracted Raman spectral parameters from both the first and second order carbon
531 peaks. Comparison of spectral parameters provide information about the structure and maturity
532 degree of the carbon (primitive and disordered carbon vs. ordered and graphitized carbon). The
533 CO3 chondrites appear to be more primitive and less thermally altered than CV3 chondrites,
534 although some CO3 chondrites are as thermal metamorphosed as the CV3 chondrites. For
535 instance, the comparison of I_D/I_G with Γ_D show that the CV3 and CO3 chondrites plot at two
536 distinct locations, apart from each other (Figure 4). The I_D/I_G ratio shows a strong positive
537 correlation with the petrologic types of meteorites (Figure 7), indicating that the intensity of the
538 D band is a good indicator of thermal metamorphism, at least for the investigated CV3 and CO3
539 chondrites.
540
541 Estimated peak metamorphic temperatures show that the studied CO3 chondrites in general
542 experienced lower temperatures than CV3 chondrites. The considered CO3 chondrites span a
543 range of 220-510 °C, whereas the CV chondrites fall between 460-636 °C. However, this
544 conclusion applies to the considered samples and not to the entire CV3 and CO3 chondrites as
545 some CO3 chondrites present higher peak metamorphic temperatures than some CV3 chondrite

(Figure 11). Indeed, there exists a CV3 chondrite (Kaba, non-Antarctic fall) whose petrologic type is lower than a CO3 chondrite (Isna, non-Antarctic find) (Bonal et al. 2016). We also observed that there is a large temperature increase between CO3.2 and CO3.4 (150 °C increase), however not much difference between CO3.4-CO3.6 (20 °C). It may be worth investigating the presence of a possible critical metamorphic temperature regime where the carbonaceous matter reaches a certain level of maturity and structural ordering of carbon, beyond which the graphitization and/or aromatization rate of carbon structures in the CO3 chondrites proceeds at a slower rate.

The oxidized CV3 chondrites ($CV3_{oxA}$ and $CV3_{oxB}$) plot apart from each other when the second order peak parameters are considered, indicating their organic matter are different to some degree. This suggests a different level of thermal metamorphism for the two subtypes in the parent body in the case of a single parent asteroid. $CV3_{oxA}$ seems to be more heated than $CV3_{oxB}$ based on the samples studied here, their average peak metamorphic temperatures were estimated as ~598-653 °C for $CV3_{oxA}$ and ~490-526 °C for $CV3_{oxB}$. A larger dataset with more samples from each subtype should be considered for more conclusive interpretations.

The three carbon thermometers available in the literature are based on the first order carbon peak parameters (e.g., Cody et al. 2008, Busemann et al. 2007; Young et al. 2020). Among the first order carbon peaks, the D band was reported to be a better tracer for thermal metamorphism. We show that the second order peak parameters present correlations with thermal metamorphism as well. Namely, the comparison of Γ_{2D} and Γ_{2D}/Γ_{D+G} presents a linear trend, and Γ_{2D} decreases while I_{2D} increases as thermal metamorphism increases (Figure 8). Because the second order

carbon peaks are observable, it would be interesting, for a future work, to create a geothermometer expression that takes into account the second order peaks as well. With a proper calibration, such a geothermometer can potentially yield more accurate peak metamorphic temperatures for the parent asteroids.

ACKNOWLEDGEMENTS

Meteorites studied in this work are recovered by the United States - Antarctic Search for Meteorites (ANSMET) program. We are very grateful to NASA Johnson Space Center and the Meteorite Working Group for generously providing the meteorite samples. We thank the associate editor Dr. Bradley De Gregorioand and the two reviewers for their helpful and constructive comments, which significantly improved this manuscript. This work is funded in part by the RISE2 node of NASA's Solar System Exploration Research Virtual Institute (SSERVI; PI: T.D. Glotch). MY acknowledges the support by the Ministry of Industry and Technology of Turkey as well as TUBITAK MAM Polar Research Institute. The data presented here will be made publicly available at Turkish Spectral Database upon publication (http://tsd.klu.edu.tr).

REFERENCES CITED

1. Alexander, C.M.O.D., Fogel, M., Yabuta, H., and Cody, G. D. (2007). The origin and evolution of chondrites recorded in the elemental and isotopic compositions of their macromolecular organic matter. Geochimica et Cosmochimica Acta, 71(17), 4380-4403.

2. Alexander, C.M.O.D., Greenwood, R.C., Bowden, R., Gibson, J.M., Howard, K.T., Franchi, I.A. (2018). A mutli-technique search for the most primitive CO chondrites. Geochimica et Cosmochimica Acta, 221,406-420.
3. Ashworth, J.R. (1980). Chondrite thermal histories: Clues from electron microscopy of orthopyroxene. Earth and Planetary Science Letters, 46(2), pp.167-177.
4. Bonal, L., Bourot-Denise, M., Quirico, E., Montagnac, G., and Lewin, E. (2007). Organic matter and metamorphic history of CO chondrites. Geochimica et Cosmochimica Acta, 71(6), 1605-1623.
5. Bonal, L., Quirico, E., Flandinet, L., and Montagnac, G. (2016). Thermal history of type 3 chondrites from the Antarctic meteorite collection determined by Raman spectroscopy of their polyaromatic carbonaceous matter. Geochimica et Cosmochimica Acta, 189, 312-337.
6. Bonal, L., Gattacceca, J., Garenne, A., Eschrig, J., Rochette, P. and Ruggiu, L.K. (2020). Water and heat: New constraints on the evolution of the CV chondrite parent body. Geochimica et Cosmochimica Acta, 276: 363-383.
7. Botta, O., and Bada, J.L. (2002). Extraterrestrial organic compounds in meteorites. Surveys in Geophysics, 23(5), 411-467.
8. Brearley, A.J. and Jones, R.H.. (1998). Chondritic meteorites. In: J.J. Papike (Ed.): Planetary materials. Reviews in Mineralogy, 36, pp.4-90.
9. Brearley A. J. (2006) The action of water. In Meteorites and the Early Solar System II D.S. Lauretta and H.Y. McSween Jr., Tucson. pp. 584–624.

612 10. Brearley, A.J. and Krot, A.N. (2013). Metasomatism in the early solar system: The record
613 from chondritic meteorites. In Metasomatism and the chemical transformation of rock
614 (pp. 659-789), Springer, Berlin, Heidelberg.
615 11. Brunetto, R., Pino, T., Dartois, E., Cao, A.T., d'Hendecourt, L., Strazzulla, G. and
616 Bréchignac, P. (2009). Comparison of the Raman spectra of ion irradiated soot and
617 collected extraterrestrial carbon. Icarus, 200(1), pp.323-337.
618 12. Busemann, H., Alexander, C.M.O.D., and Nittler, L.R. (2007). Characterization of
619 insoluble organic matter in primitive meteorites by microRaman
620 spectroscopy. Meteoritics & Planetary Science, 42(7-8), 1387-1416.
621 13. Cody, G.D., Alexander, C.M.O.D., Yabuta, H., Kilcoyne, A.L.D., Araki, T., Ade, H.,
622 Dera, R., Fogel, M., Militzer, B. and Mysen, B.O. (2008) Organic thermometry for
623 chondritic parent bodies. Earth and Planetary Science Letters 272, 446-455.
624 14. Ferrari, A.C., and Robertson, J. (2000). Interpretation of Raman spectra of disordered and
625 amorphous carbon. Physical review B, 61(20), 14095.
626 15. Ferrari, A.C., and Robertson, J. (2001). Resonant Raman spectroscopy of disordered,
627 amorphous, and diamondlike carbon. Physical review B, 64(7), 075414.
628 16. Gattacceca, J., Bonal, L., Sonzogni, C., and Longerey, J. (2019). CV Chondrites: More
629 than One Parent Body, 2157, In 82nd Annual Meeting of The Meteoritical Society.
630 17. Greenwood, R.C., and Franchi, I.A. (2004). Alteration and metamorphism of CO3
631 chondrites: Evidence from oxygen and carbon isotopes. Meteoritics & Planetary Science,
632 39(11), 1823-1838.

18. Howard, K.T., Benedix, G.K., Bland, P.A., and Cressey, G. (2010). Modal mineralogy of CV3 chondrites by X-ray diffraction (PSD-XRD). Geochimica et Cosmochimica Acta, 74(17), 5084-5097.

19. Huss, G.R., Rubin, A.E., and Grossman, J.N. (2006). Thermal metamorphism in chondrites. Meteorites and the early solar system II, 943, pp. 567-586.

20. Itoh, D., and Tomeoka, K. (2003). Dark inclusions in CO3 chondrites: New indicators of parent-body processes. Geochimica et Cosmochimica Acta, 67(1), 153-169.

21. Jenniskens P., Fries M.D., Yin Q.-Z., Zolensky M., Krot A.N., Sandford S.A., Sears D., Beauford R., Ebel D.S., Friedrich J.M., and others. (2012). Radar-Enabled Recovery of the Sutter's Mill Meteorite, a Carbonaceous Chondrite Regolith Breccia. Science 338:1583–1587.

22. Keck B. D. and Sears D. W. G. (1987). Chemical and physical studies of type 3 chondrites VIII: The CO chondrites. Geochimica et Cosmochimica Acta 51:3013–3022.

23. Kessel, R., Beckett, J.R. and Stolper, E.M. (2007). The thermal history of equilibrated ordinary chondrites and the relationship between textural maturity and temperature. Geochimica et Cosmochimica Acta, 71(7), pp.1855-1881.

24. Kitajima, F., Nakamura, T., Takaoka, N., and Murae, T. (2002). Evaluating the thermal metamorphism of CM chondrites by using the pyrolytic behavior of carbonaceous macromolecular matter. Geochimica et Cosmochimica Acta, 66(1), 163-172.

25. Krot, A.N., Scott, E.R.D., and Zolensky, M.E. (1995). Mineralogic and chemical variations among CV3 chondrites and their components: Nebular and asteroidal processing. Meteoritics, 30, 748-775.

655 26. Krot, A.N., Petaev, M.I., Scott, E.R., Choi, B.G., Zolensky, M.E., and Keil, K. (1998).
656 Progressive alteration in CV3 chondrites: More evidence for asteroidal alteration.
657 Meteoritics & Planetary Science, 33(5), 1065-1085.
658 27. Krot, A.N., Petaev, M.I., and Bland, P.A. (2003). Growth of ferrous olivine in the
659 oxidized CV chondrites during a fluid-assisted thermal metamorphism.
660 Meteoritics & Planetary Science, 38, A73.
661 28. Krot, A.N., Keil, K., Scott, E.R.D., Goodrich, C.A. and Weisberg, M.K. (2014).
662 Classification of meteorites and their genetic relationships. Meteorites and
663 Cosmochemical Processes, Volume 1 of Treatise on Geochemistry (Second Edition).
664 Elsevier, 2014. Edited by Andrew M. Davis, p.1-63.
665 29. Lunning, N.G., Corrigan, C.M., McSween Jr, H.Y., Tenner, T.J., Kita, N.T., and Bodnar,
666 R.J. (2016). CV and CM chondrite impact melts. Geochimica et Cosmochimica Acta,
667 189, 338-358.
668 30. Ma, B., Rodriguez, R.D., Ruban, A., Pavlov, S., and Sheremet, E. (2019). The correlation
669 between electrical conductivity and second-order Raman modes of laser-reduced
670 graphene oxide. Physical Chemistry Chemical Physics, 21(19), 10125-10134.
671 31. MacPherson, G.J. and Krot, A.N. (2014). The formation of Ca-, Fe-rich silicates in
672 reduced and oxidized CV chondrites: the roles of impact-modified porosity and
673 permeability, and heterogeneous distribution of water ices. Meteoritics & Planetary
674 Science, 49(7), pp.1250-1270.
675 32. McSween Jr, H.Y. (1977a). Carbonaceous chondrites of the Ornans type: A metamorphic
676 sequence. Geochimica et Cosmochimica Acta, 41(4), pp.477-491.

677 33. McSween Jr, H.Y. (1977b). Chemical and petrographic constraints on the origin of
678 chondrules and inclusions in carbonaceous chondrites. Geochimica et Cosmochimica
679 Acta, 41(12), 1843-1860.
680 34. McSween Jr, H.Y. (1977c). Petrographic variations among carbonaceous chondrites of
681 the Vigarano type. Geochimica et Cosmochimica Acta, 41(12), 1777-1790.
682 35. Nakato, A., Nakamura, T., Kitajima, F., and Noguchi, T. (2008). Evaluation of
683 dehydration mechanism during heating of hydrous asteroids based on mineralogical and
684 chemical analysis of naturally and experimentally heated CM chondrites. Earth, Planets
685 and Space, 60(8), 855-864.
686 36. Németh, P., and Garvie, L.A. (2020). Extraterrestrial, shock-formed, cage-like
687 nanostructured carbonaceous materials. American Mineralogist, 105(2), 276-281.
688 37. Pizzarello, S., Cooper, G.W., and Flynn, G. J. (2006). The nature and distribution of the
689 organic material in carbonaceous chondrites and interplanetary dust particles. Meteorites
690 and the early solar system II, 1, 625-651.
691 38. Quirico E., Raynal P. I. and Bourot-Denise M. (2003) Metamorphic grade of organic
692 matter in six unequilibrated ordinary chondrites. Meteoritics & Planetary Science, 38,
693 795–811.
694 39. Quirico, E., Bonal, L., Beck, P., Yabuta, H., Nakamura, T., Nakato, A., Flandinet, L.,
695 Montagnac, G., Schmitt-Kopplin, P. and Herd, C.D.K. (2018). Prevalence and nature of
696 heating processes in CM and C2-ungrouped chondrites as revealed by insoluble organic
697 matter. Geochimica et Cosmochimica Acta, 241, pp.17-37.
698 40. Remusat, L. (2014). Organic material in meteorites and the link to the origin of life.
699 In BIO web of conferences (Vol. 2, p. 03001). EDP Sciences.

700 41. Rubin, A.E. (1995). Petrologic evidence for collisional heating of chondritic
701 asteroids. Icarus, 113(1), 156-167.
702 42. Sadezky, A., Muckenhuber, H., Grothe, H., Niessner, R. and Pöschl, U. (2005). Raman
703 microspectroscopy of soot and related carbonaceous materials: spectral analysis and
704 structural information. Carbon, 43(8), pp.1731-1742.
705 43. Scott, E.R.D., Krot, A. N. (2007). In Treatise on Geochemistry, eds H. D. Holland, K. K.
706 Turekian, Eds. (Elsevier Pergamon, Oxford), vol. 1, pp. 1–72.
707 44. Sears, D.W. (2016). The CO chondrites: Major recent Antarctic finds, their thermal and
708 radiation history, and describing the metamorphic history of members of the
709 class. Geochimica et Cosmochimica Acta, 188, 106-124.
710 45. Starkey, N.A., Franchi, I.A., and Alexander, C.O.D. (2013). A Raman spectroscopic
711 study of organic matter in interplanetary dust particles and meteorites using multiple
712 wavelength laser excitation. Meteoritics & Planetary Science, 48(10), 1800-1822.
713 46. Suzuki, A., Yamanoi, Y., Nakamura, T., and Nakashima, S. (2010). Micro-spectroscopic
714 characterization of organic and hydrous components in weathered Antarctic
715 micrometeorites. Earth, planets and space, 62(1), 33-46.
716 47. Tuinstra, F., and Koenig, J.L. (1970). Raman spectrum of graphite. The Journal of
717 chemical physics, 53(3), 1126-1130.
718 48. Vollebregt, S., Ishihara, R., Tichelaar, F.D., Hou, Y., and Beenakker, C.I.M. (2012).
719 Influence of the growth temperature on the first and second-order Raman band ratios and
720 widths of carbon nanotubes and fibers. Carbon, 50(10), 3542-3554.
721 49. Weisberg, M.K., Prinz, M., Clayton, R.N., and Mayeda, T.K. (1997). CV3 chondrites:
722 Three subgroups, not two. Meteoritics and Planetary Science Supplement, 32, 138–139.

50. Weisberg, M.K., McCoy, T.J., and Krot, A.N. (2006). Systematics and evaluation of meteorite classification. Meteorites and the early solar system II.

51. Yesiltas, M., Kebukawa, Y., Peale, R.E., Mattson, E., Hirschmugl, C.J., and Jenniskens, P. (2014). Infrared imaging spectroscopy with micron resolution of Sutter's Mill meteorite grains. Meteoritics & Planetary Science, 49(11), 2027-2037.

52. Yesiltas, M. (2018a). Investigation of carbon in the Allan Hills A77278 meteorite via 2D and 3D Raman microspectroscopy. Journal of Raman Spectroscopy, 49(11), 1812-1821.

53. Yesiltas, M. (2018b). Investigation of carbonates in the Sutter's Mill meteorite grains with hyperspectral infrared imaging micro-spectroscopy. Spectrochimica Acta Part A: Molecular and Biomolecular Spectroscopy, 194, 92-101.

54. Yesiltas, M., Glotch, T.D., Jaret, S., Verchovsky, A.B. and Greenwood, R.C. (2019). Carbonaceous matter in the Sariçiçek meteorite. Meteoritics & Planetary Science, 54(7), pp.1495-1511.

55. Young, J., Yesiltas, M., Glotch, T.D. (2020). Reconstructing parent body metamorphism via raman spectroscopy of organic materials in ordinary chondrites. Meteoritics & Planetary Science, in review.

56. Zolensky, M., Barrett, R. and Browning, L., 1993. Mineralogy and composition of matrix and chondrule rims in carbonaceous chondrites. Geochimica et Cosmochimica Acta, 57(13), pp.3123-3148.

Figure captions

Figure 1. Two dimensional carbon distribution maps of studied CV3 (top, black panel) and CO3 (bottom, red panel) chondrites. The numbers on each image denotes the meteorite sample listen in Table 1.

Figure 2. Raman spectra extracted from carbon-rich locations within the measured area of each meteorite.

748 **Figure 3.** Lorentzian fit procedure example for a single-pixel Raman spectrum. The spectrum
749 contains first order (D and G) bands as well as second order (2D and D+G) carbon peaks. Gray
750 solid lines are individual fits while the black solid line is the actual collected spectrum. Vertical
751 gray dashed lines indicate the positions of peaks.

752 **Figure 4.** Peak intensity ratios of the studied meteorites vs. width of the D (a) and G (b) bands.

753 **Figure 5.** Comparison of width and position for the first order D (a) and G (b) bands.

754 **Figure 6.** First order width ratios Γ_D/Γ_G vs. width of D (a) and G (b) bands.

755 **Figure 7.** Petrologic types of the studied meteorites vs. their first order peak intensity ratios (a)
756 and width of the D band (b).

757 **Figure 8.** Comparison of Γ_{2D} (width of 2D band) with Γ_{2D}/Γ_{D+G} (ratio of second order peak
758 widths, a) and I_{2D}/I_{D+G} (peak intensity ratios of second order peaks, b).

759 **Figure 9.** Comparison of first order peak intensity ratios with widths of second order peaks 2D
760 band (a) and D+G band (b).

761 **Figure 10.** a: Comparison of Γ_D (width of the D band) with ω_{D+G} (position of the D+G band). b:
762 Comparison of second order peak intensity values (I_{2D}/I_{D+G}).

763 **Figure 11.** Peak metamorphic temperatures of CV3 and CO3 chondrites estimated using
764 thermometric equations of Busemann et al. (2007), Cody et al. (2008), and Young et al. (2020).
765 The top left portion of the data is shown in the inset in the lower left.

766 **Figure 12.** Calculated K_T values of the investigated CV3 chondrites, following the method
767 described in Young et al. (2020).

Figure 1

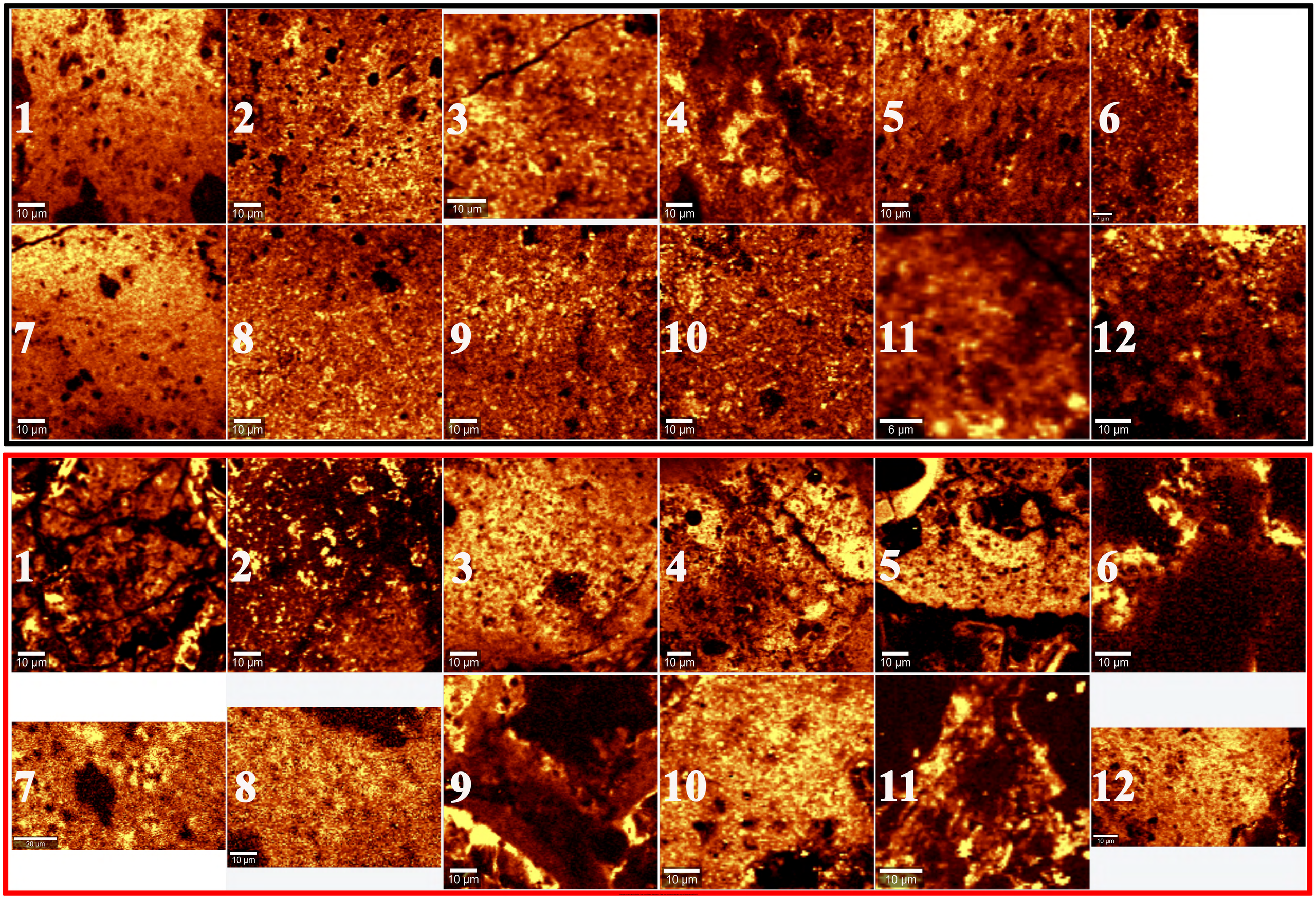

Figure 2

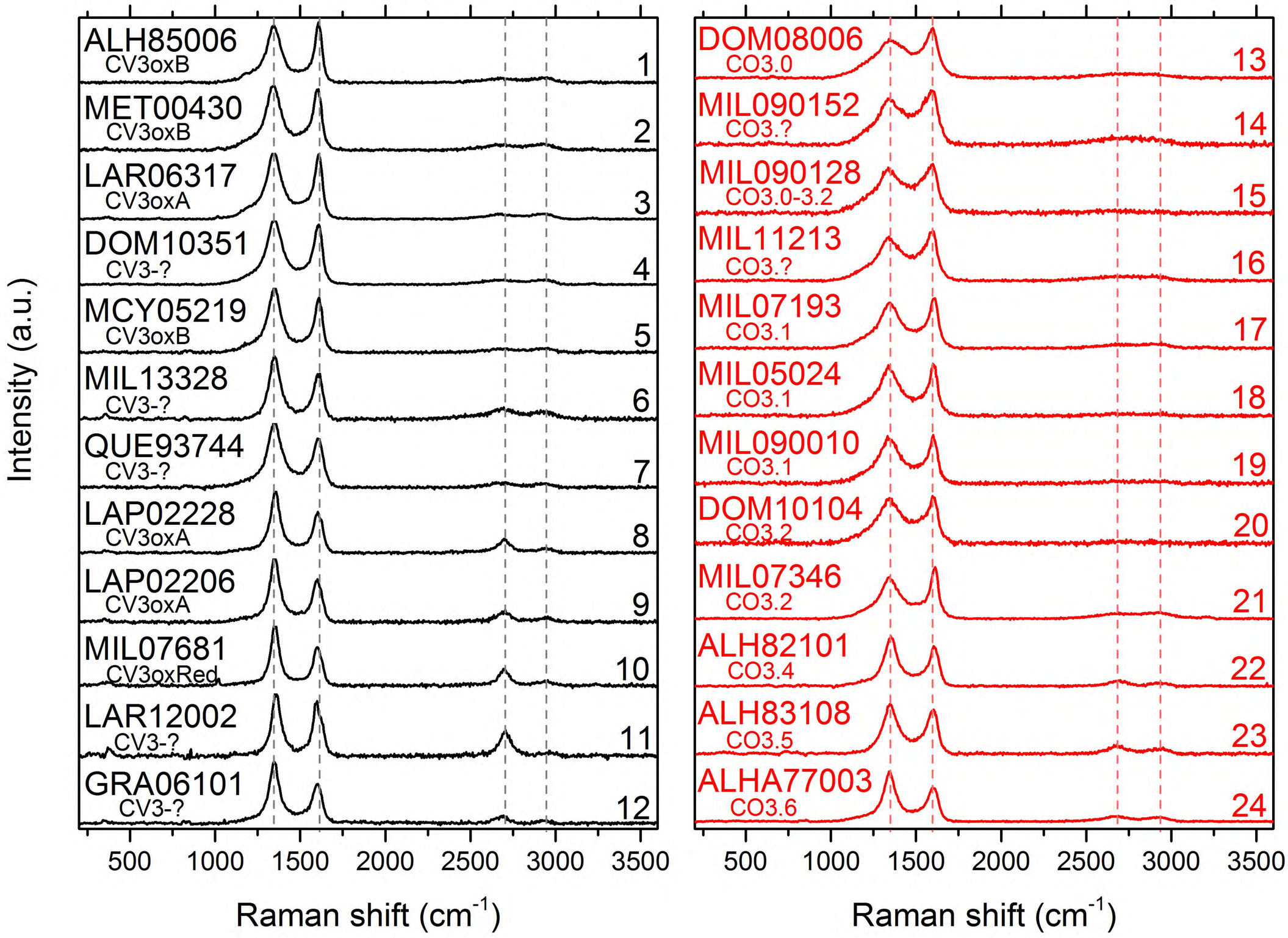

Figure 3

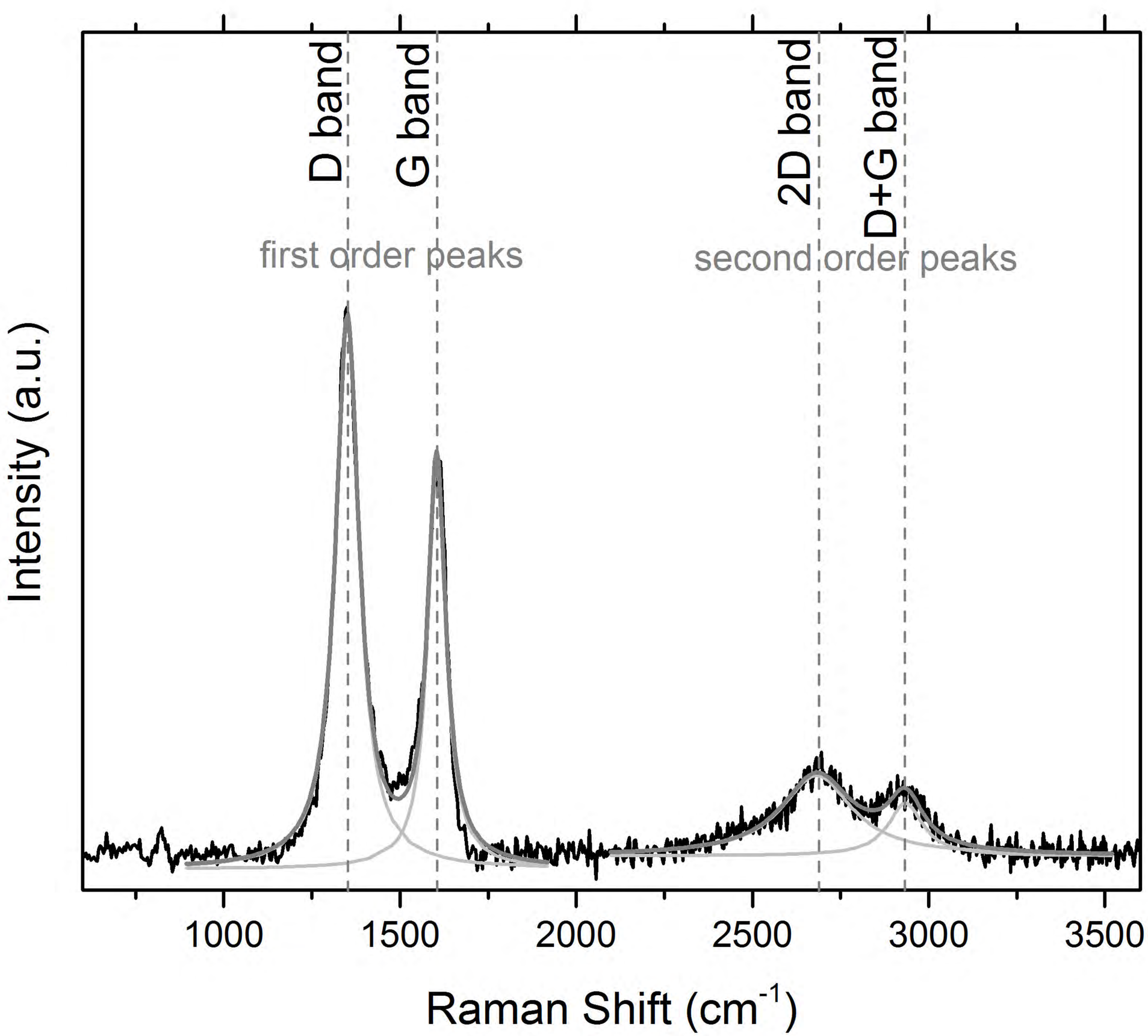

Figure 4

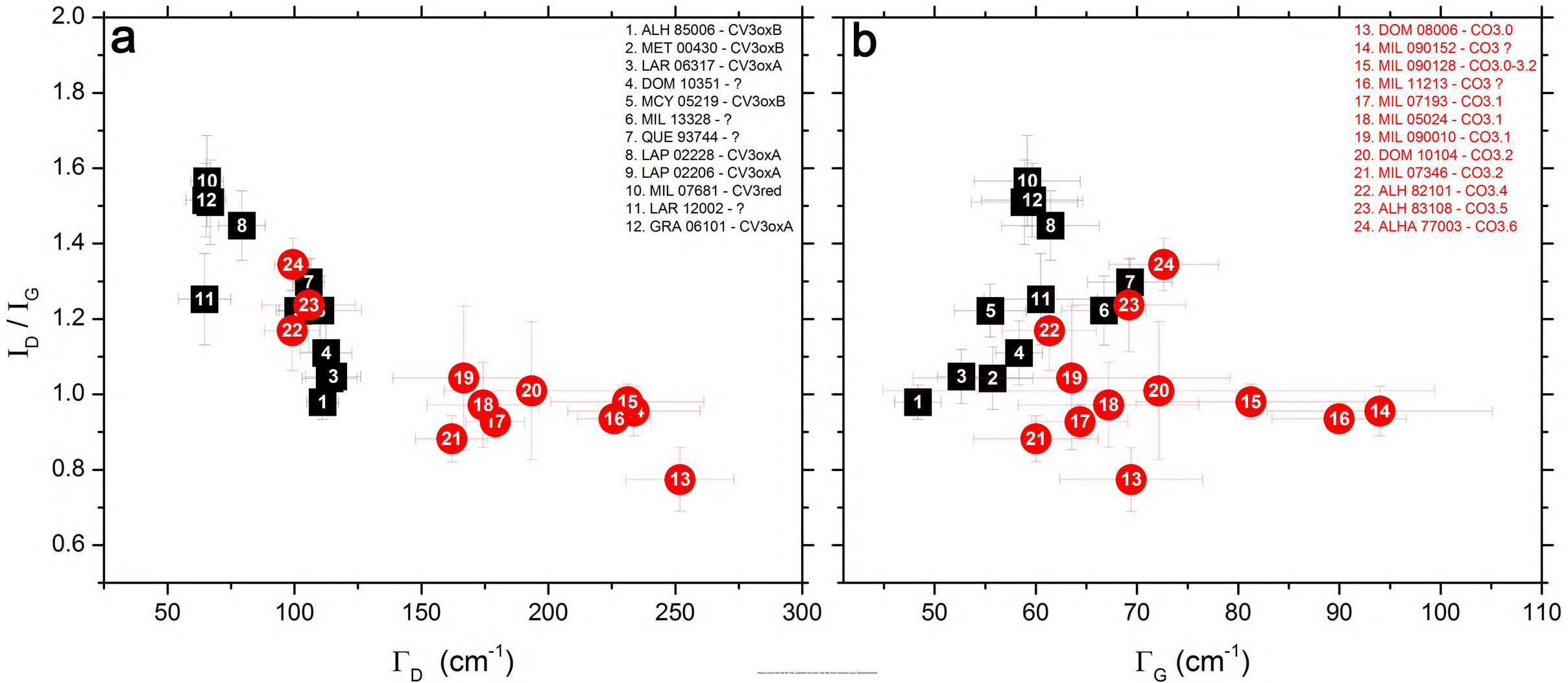

Figure 5

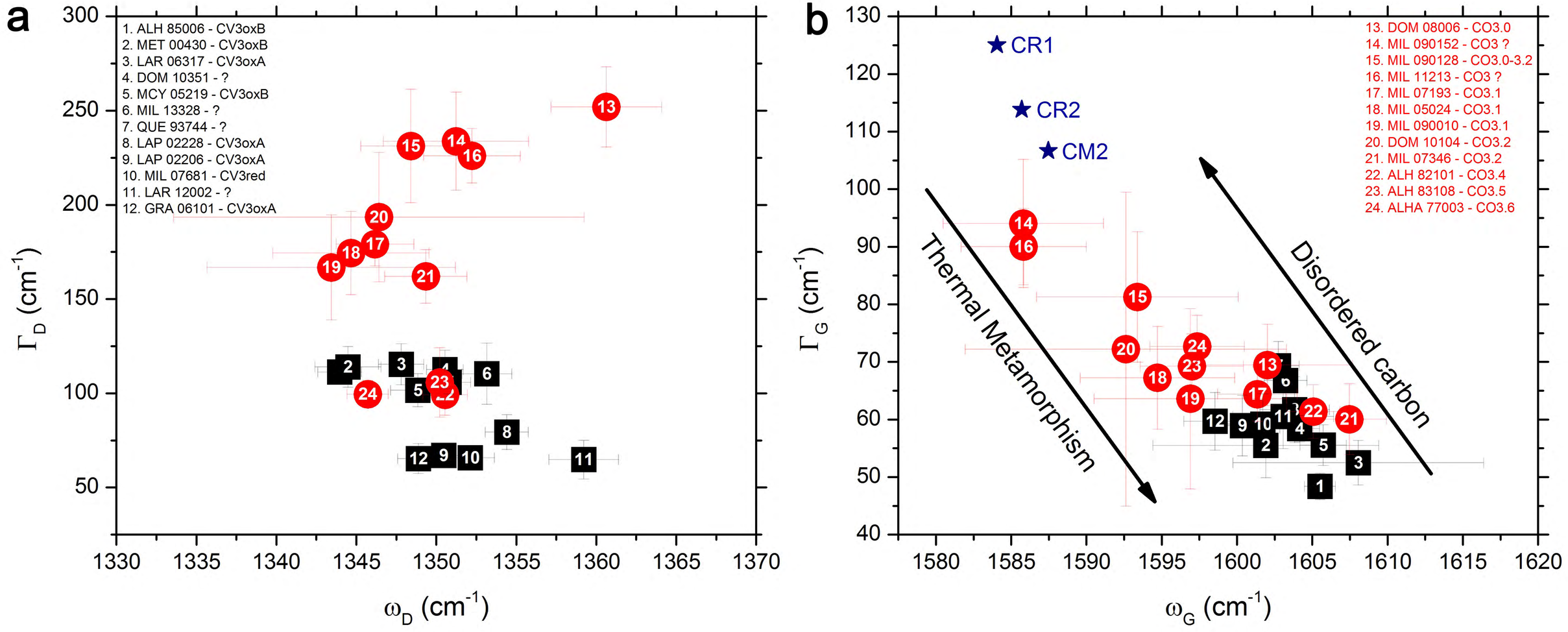
a
1. ALH 85006 - CV3oxB
2. MET 00430 - CV3oxB
3. LAR 06317 - CV3oxA
4. DOM 10351 - ?
5. MCY 05219 - CV3oxB
6. MIL 13328 - ?
7. QUE 93744 - ?
8. LAP 02228 - CV3oxA
9. LAP 02206 - CV3oxA
10. MIL 07681 - CV3red
11. LAR 12002 - ?
12. GRA 06101 - CV3oxA
Γ_D (cm^{-1})
ω_D (cm^{-1})
b
CR1
CR2
CM2
13. DOM 08006 - CO3.0
14. MIL 090152 - CO3 ?
15. MIL 090128 - CO3.0-3.2
16. MIL 11213 - CO3 ?
17. MIL 07193 - CO3.1
18. MIL 05024 - CO3.1
19. MIL 090010 - CO3.1
20. DOM 10104 - CO3.2
21. MIL 07346 - CO3.2
22. ALH 82101 - CO3.4
23. ALH 83108 - CO3.5
24. ALHA 77003 - CO3.6
Thermal Metamorphism
Disordered carbon
Γ_G (cm^{-1})
ω_G (cm^{-1})

Figure 6

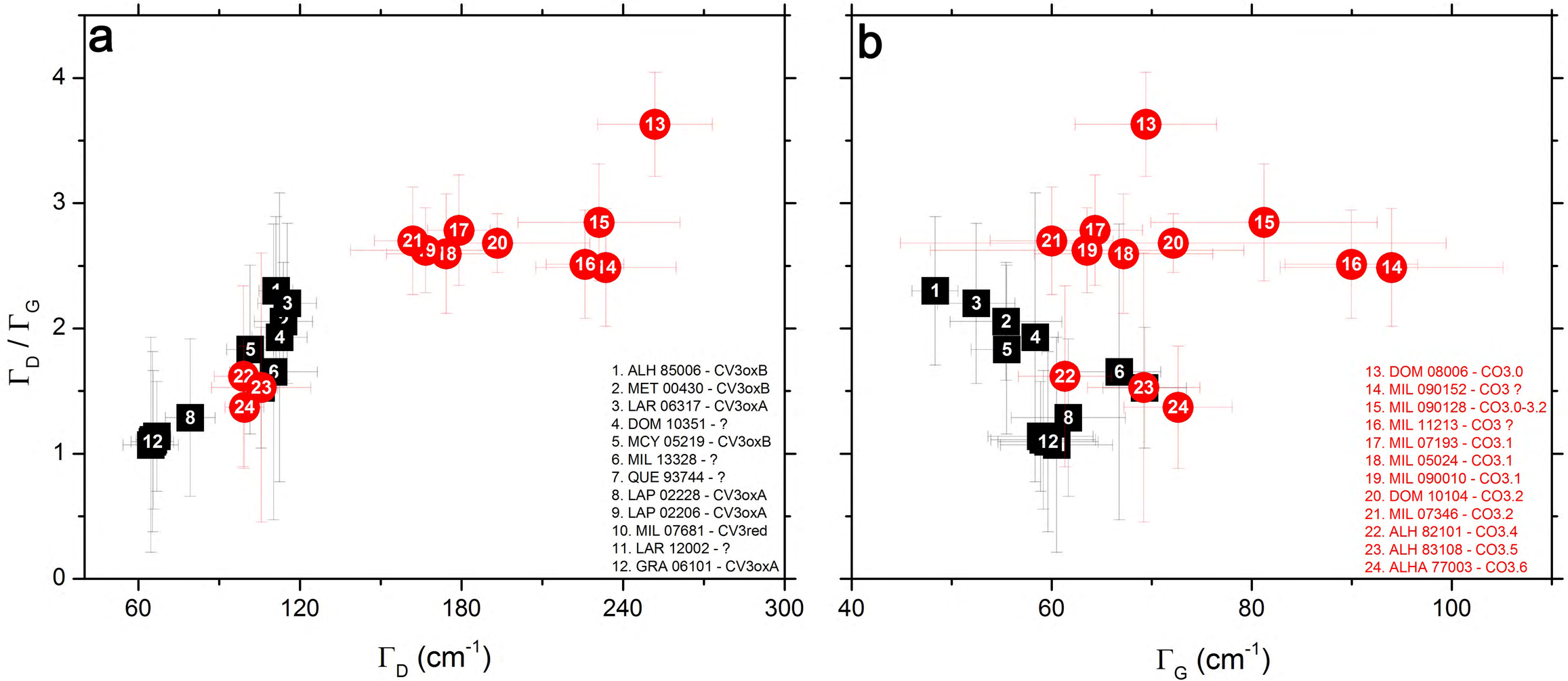

Figure 7

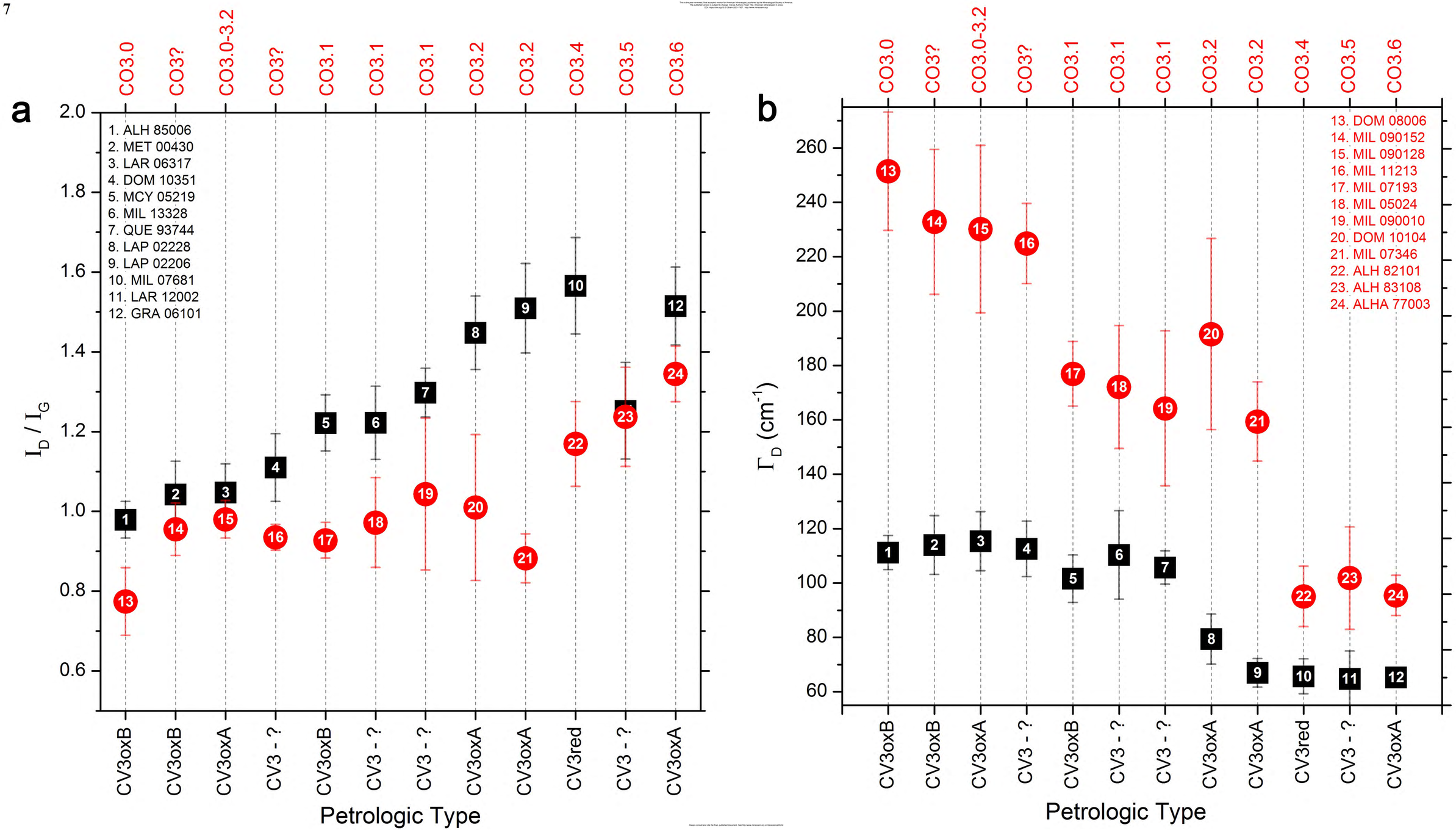
a
b
CO3.0
CO3?
CO3.0-3.2
CO3?
CO3.1
CO3.1
CO3.1
CO3.2
CO3.2
CO3.4
CO3.5
CO3.6
1. ALH 85006
2. MET 00430
3. LAR 06317
4. DOM 10351
5. MCY 05219
6. MIL 13328
7. QUE 93744
8. LAP 02228
9. LAP 02206
10. MIL 07681
11. LAR 12002
12. GRA 06101
13. DOM 08006
14. MIL 090152
15. MIL 090128
16. MIL 11213
17. MIL 07193
18. MIL 05024
19. MIL 090010
20. DOM 10104
21. MIL 07346
22. ALH 82101
23. ALH 83108
24. ALHA 77003
I_D / I_G
Γ_D (cm^-1)
CV3oxB
CV3oxB
CV3oxA
CV3 - ?
CV3oxB
CV3 - ?
CV3 - ?
CV3oxA
CV3oxA
CV3red
CV3 - ?
CV3oxA
Petrologic Type

Figure 8

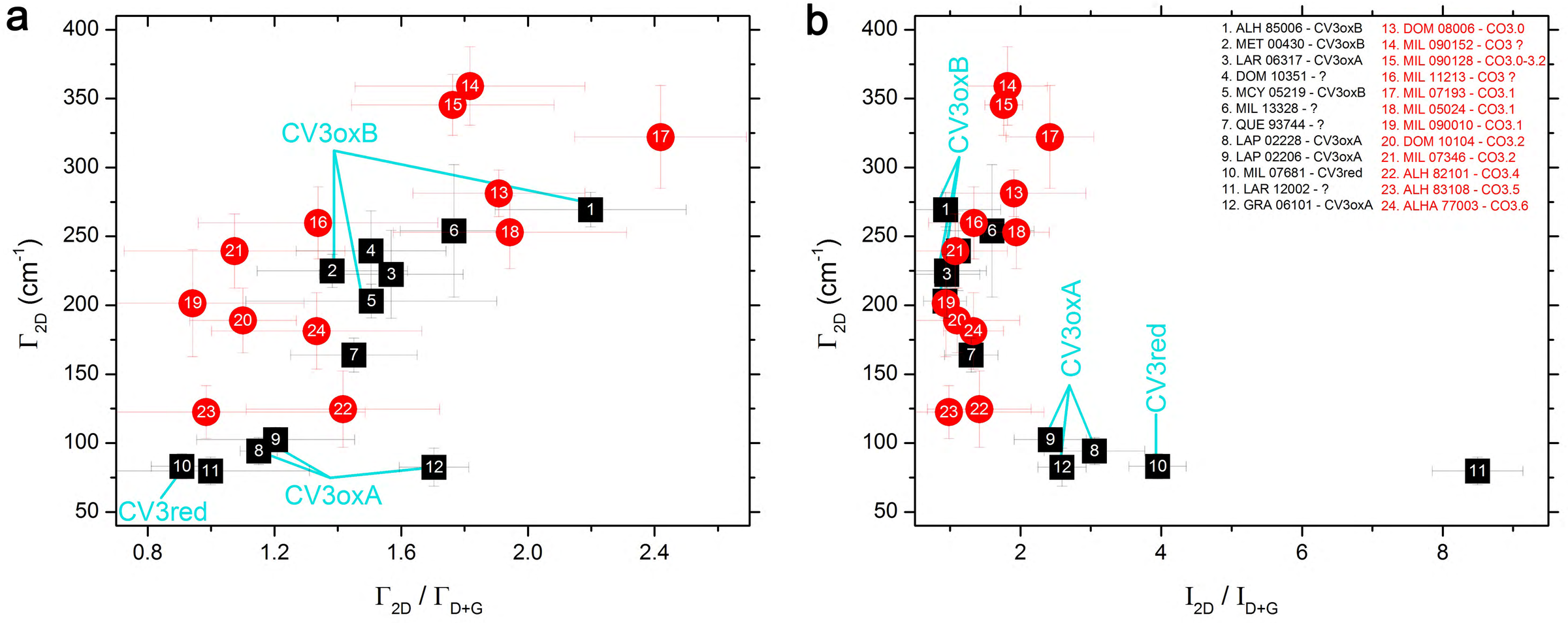

Figure 9

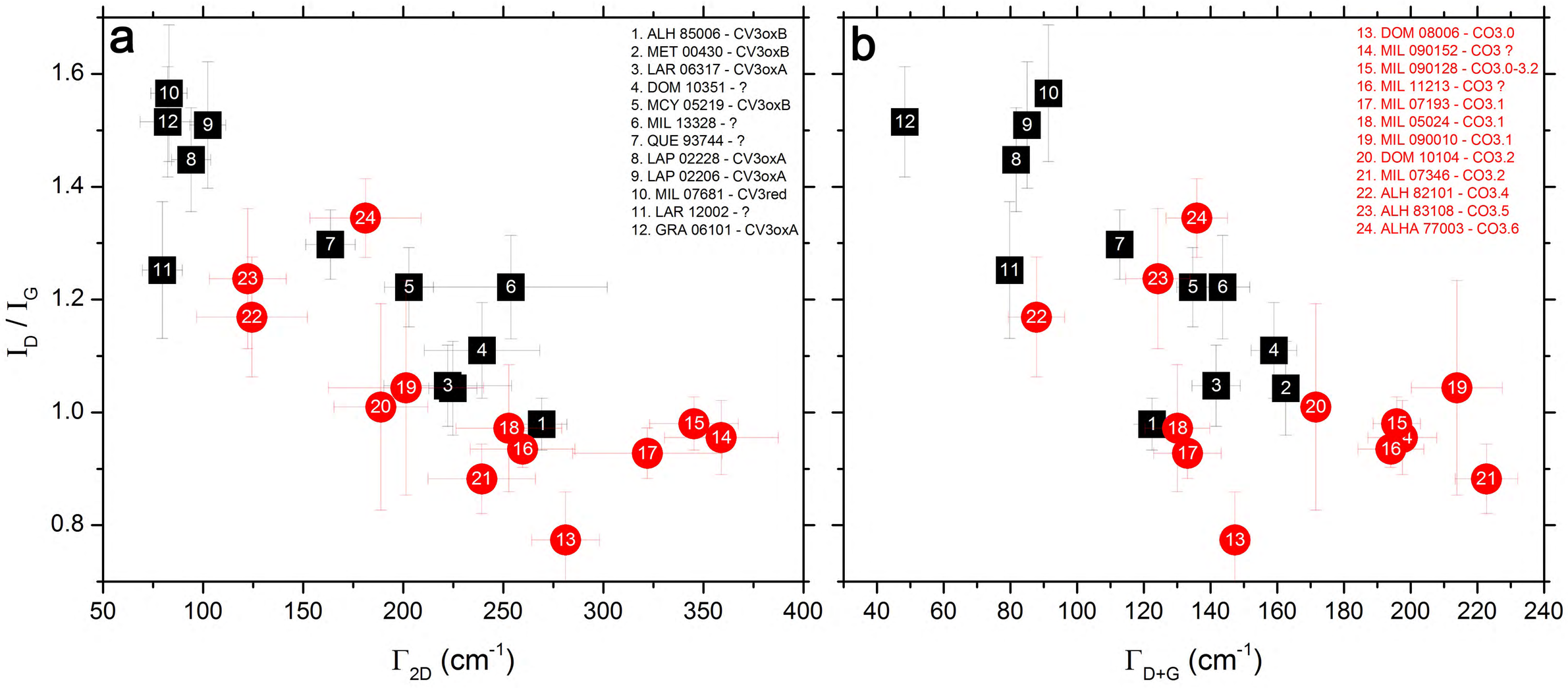

Figure 10

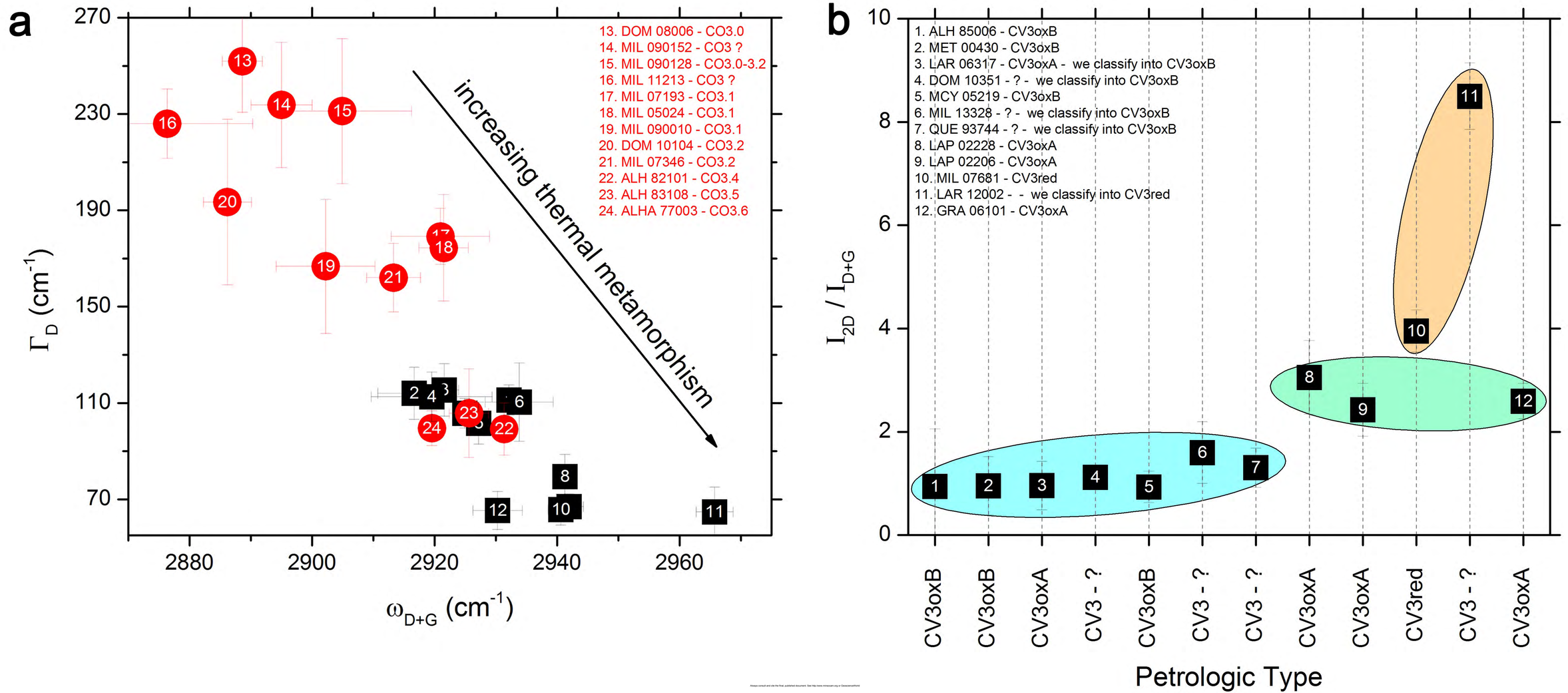
a
13. DOM 08006 - CO3.0
14. MIL 090152 - CO3 ?
15. MIL 090128 - CO3.0-3.2
16. MIL 11213 - CO3 ?
17. MIL 07193 - CO3.1
18. MIL 05024 - CO3.1
19. MIL 090010 - CO3.1
20. DOM 10104 - CO3.2
21. MIL 07346 - CO3.2
22. ALH 82101 - CO3.4
23. ALH 83108 - CO3.5
24. ALHA 77003 - CO3.6
increasing thermal metamorphism
Γ_D (cm^{-1})
ω_{D+G} (cm^{-1})
270
230
190
150
110
70
2880
2900
2920
2940
2960
b
1. ALH 85006 - CV3oxB
2. MET 00430 - CV3oxB
3. LAR 06317 - CV3oxA - we classify into CV3oxB
4. DOM 10351 - ? - we classify into CV3oxB
5. MCY 05219 - CV3oxB
6. MIL 13328 - ? - we classify into CV3oxB
7. QUE 93744 - ? - we classify into CV3oxB
8. LAP 02228 - CV3oxA
9. LAP 02206 - CV3oxA
10. MIL 07681 - CV3red
11. LAR 12002 - - we classify into CV3red
12. GRA 06101 - CV3oxA
I_{2D} / I_{D+G}
0
2
4
6
8
10
CV3oxB
CV3oxB
CV3oxA
CV3 - ?
CV3oxB
CV3 - ?
CV3 - ?
CV3oxA
CV3oxA
CV3red
CV3 - ?
CV3oxA
Petrologic Type

Figure 11

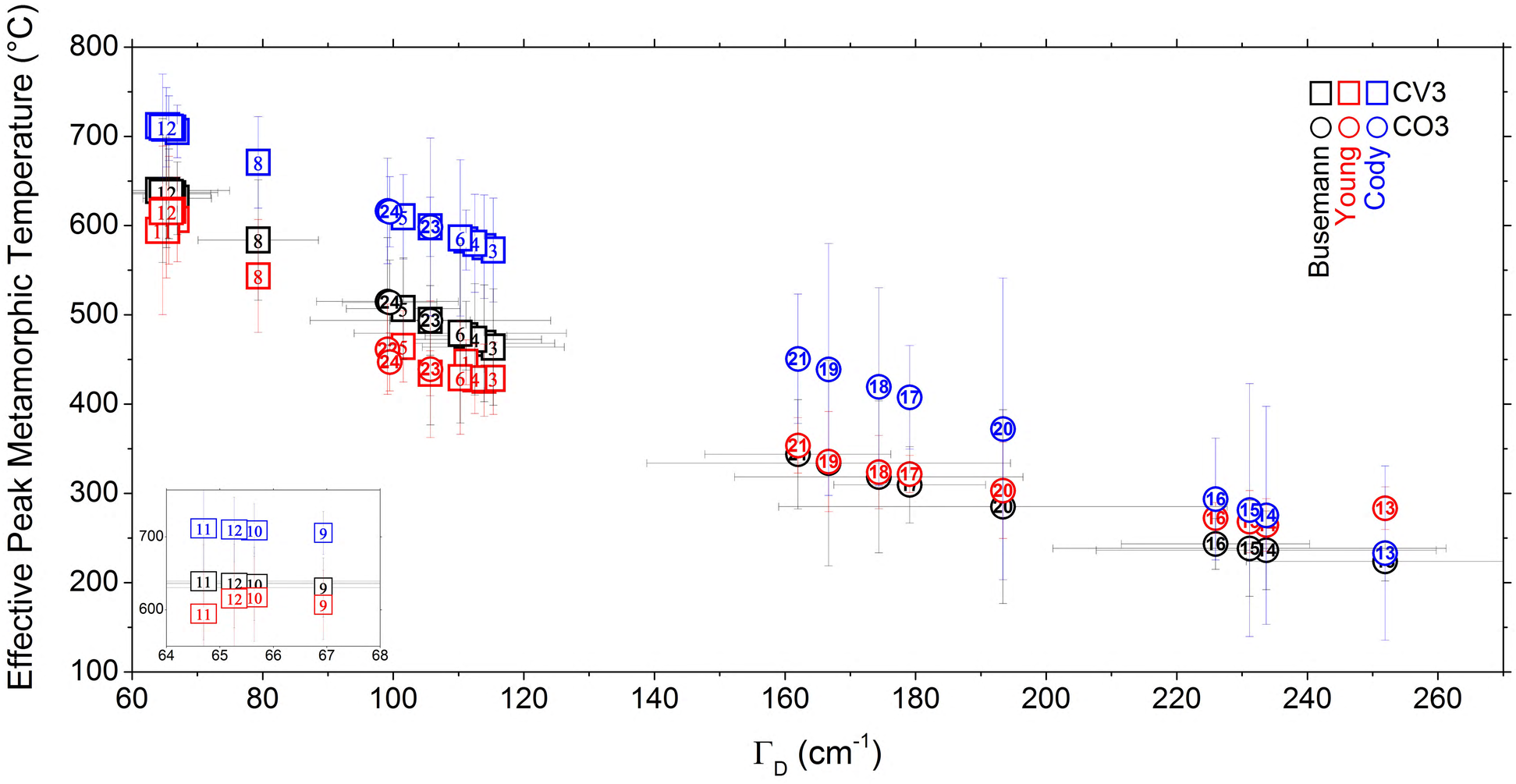
Effective Peak Metamorphic Temperature (°C)
Γ_D (cm^{-1})
CV3
CO3
Busemann
Young
Cody

Figure 12